Experimental evidence and theoretical criteria for a local-field rotational correlation length in metallic spin glasses

Dojun Youm and Sheldon Schultz
Department of Physics, University of California, San Diego, California 92093
(Received 28 October 1985)

Detailed measurements of the temperature and field dependence of the ac susceptibility χ for the spin glass Cu-Mn$_x$ reveal a new cusp transition whose locus is a line in the χ-T plane, independent of x. We have formulated a modified mean-field theory incorporating spin clusters whose parameters are deduced from a fit to the data. We find a correlation length associated with the rotational coherence of the local field and identify the cusp line as a physical feature corresponding to the divergence of the correlation length at the transition temperature T_g. We find that our data are well represented by scaling relations both above and below T_g, and from these relations we evaluate the critical exponents δ, γ, δ', and γ'.

I. INTRODUCTION

There have been numerous theoretical and experimental studies of the physical properties of metallic spin glasses in an attempt to identify features which might be the signature of a phase transition.[1] We believe that our extended data of the dc magnetic field and temperature dependence of the parallel ac susceptibility, $\chi(H,T)$, reveal a new general feature, and we present a theoretical development in which we find a correlation length associated with the rotational coherence of the random local fields. We identify a transition as occurring at the temperature at which the correlation length diverges. Using model parameters fitted to our susceptibility data, we are able to predict the temperature and field dependence of the transition. We find satisfactory agreement with the observed feature, which leads us to suggest that although our model is necessarily a simplification of the true spin glass, our basic physical assumptions, and the new correlation length we identify, must contain the most significant features of an eventual, more exact treatment. We suggest that a large spin or cluster formulation is inherent to a satisfactory explanation of the suppression of χ by weak dc fields[2] and that the inclusion of the cluster rotational response to perturbing ac fields and the consequent rotational correlation between clusters, as illustrated in our theory, should be incorporated in future formulations.

We find that the dc field and temperature dependence of χ are well represented by suitable scaling relations chosen for the conditions $T > T_g^0$ and $T < T_g^0$, respectively. From these scaling relations we recover the critical exponents δ and γ both above and below T_g.

II. EXPERIMENTAL DATA

In Fig. 1 we present the parallel ac susceptibility, $\chi = dM/dh$, as a function of temperature T for fixed values of applied dc magnetic field, H. M is the magnetization and h is an applied 30-Hz ac field. There are several important aspects of these data.

(1) When $H = 0$, the data correspond to the well-known cusp[3] in χ with peak value χ^0 at the temperature T_g^0.

(2) When there is a modest applied dc field, $H \approx 100$ G, there is a large suppression of χ near T_g^0 which appears as a rounding of the cusp, as previously reported in the literature.[4,5]

(3) For larger values of H we observe new important features; (i) As T is reduced from above T_g^0, the suscepti-

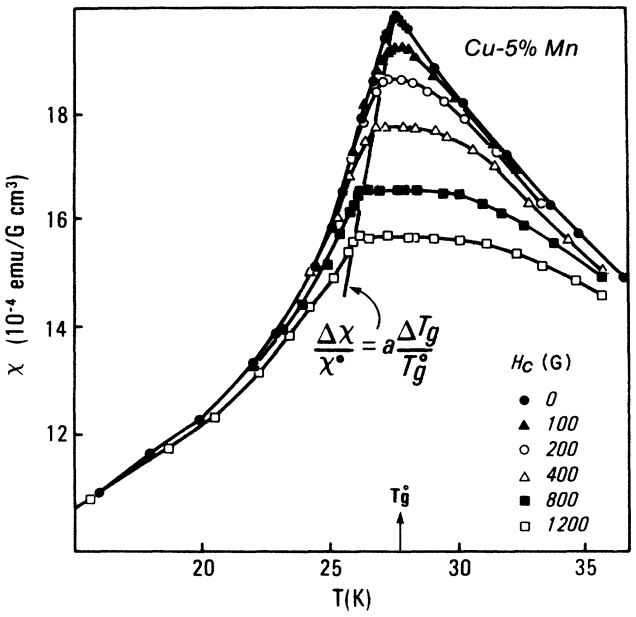

FIG. 1. The parallel ac susceptibility of a 5 at. % Cu-Mn foil as a function of temperature for several values of applied dc magnetic field, H. For weak fields, there is a large suppression of χ near T_g, but the data appear to be a rounding of the cusp. For larger values of H (≥ 400 G) there is a temperature-independent region, terminating at low T with a well-defined discontinuity. The locus of these points of discontinuity are well represented by a straight line with $\Delta\chi/\chi^0 = a\Delta T_g/T_g^0$. Values of the slope, a, for several spin-glass alloys are presented in Table I.

bility smoothly becomes less T dependent, with many samples actually exhibiting a flat, almost T-independent behavior[6–8] before terminating in an abrupt change of slope at a well-defined temperature, $T_g(H)$. (ii) The locus of the $T_g(H)$ so determined are straight lines for H up to ~ 1000 G. In larger fields the locus of $T_g(H)$ exhibits curvature.[9] We shall refer to the initial linear part of the observed discontinuity as the cusp line.

(4) If we define $\Delta T_g = T_g(H) - T_g^0$, and $\Delta\chi = \chi\{T_g(H)\} - \chi^0$, we find that for $0.2 \leq H \leq 1.2$ kG, $\Delta\chi/\chi^0 = a\Delta T_g/T_g^0 = bH^c$ with the values of a, b, and c as given in Table I.

In Fig. 2(a) we plot χ as a function of magnetic field for several temperatures above T_g^0. We find that $\chi(T,0) - \chi(T,H)$ satisfies the well-known scaling relation[10] as shown in Fig. 2(b). The values of δ and γ which we obtain are 3 ± 0.8 and 1.85 ± 0.5, respectively. In Fig. 3(a) we also plot χ as a function of magnetic field but for several values of temperature below T_g^0. We find that the data are well represented by an even simpler scaling relation of the form,

$$\chi(H,T) - \chi(0,T) = f(H^{\delta'/2}/(T_g^0 - T)^{\gamma'}) = f(H/(T_g^0 - T)),$$

as shown in Fig. 3(b). That is, we see that the data below T_g^0 are very well fitted by $\delta' = 2$ and $\gamma' = 1$.

We have taken the data below T_g by the following two sequences in order to check whether there were cooling rates or other effects which might indicate potential relaxation problems. In sequence 1, we cooled in a fixed dc field, stopping to stabilize the temperature at each value, and taking several minutes to establish a given data point. The cooling rates were set by various thermal time constants inherent to the masses of the shield, etc. One can see the typical temperature spacing between points from the data of Fig. 1. In sequence 2, we slowly cooled below T_g in zero field, and then having stabilized at a given temperature, raised the dc field to the levels indicated in Figs. 1 and 3. We found that after changing to a given dc field level, it took approximately 5–10 min before we had a time-invariant signal. (It is not known what the physical origins of the small signal variations during this period were.) Once the signals settled down, we found that the values agreed with those obtained by sequence 1 to within the experimental uncertainties. Thus we suggest that at least for the ac susceptibility, the data should be representative of an equilibrium configuration for the temperature and field range studied. Although we did make preliminary measurements at frequencies of 10^{-3} and 700 Hz which indicated that the cusp line of Fig. 1 was not strongly affected, we believe a future, full study of frequency and time effects is warranted.

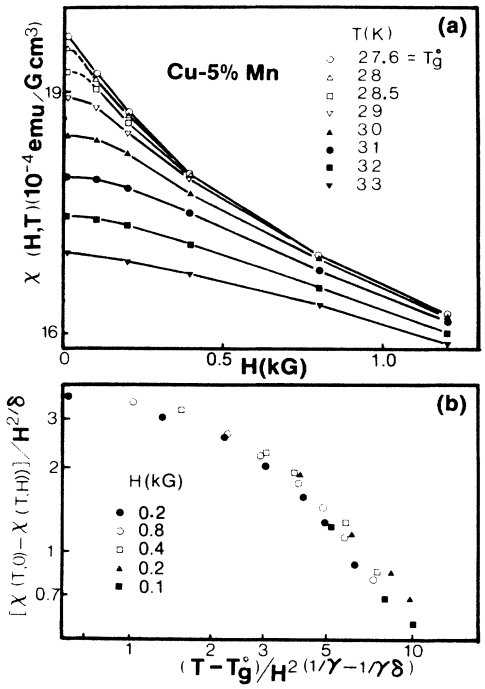

FIG. 2. In (a) the ac susceptibility data of Fig. 1 are replotted as a function of dc magnetic field for several values of temperature (all above T_g^0). In the vicinity of $H = 0$ and $T = T_g^0$ we note that the curvature would exhibit a singularity as in the solution of Sherrington and Kirkpatrick (Ref. 16). In (b) we replot the data using the scaled axis as shown. The values of γ and δ are given in the text.

TABLE I. Properties of cusp line. $\Delta\chi/\chi^0 = a\Delta T_g/T_g^0 \approx b(H/H_0)^c$, $H_0 = 1$ kG for $0.2 < H < 1.2$ kG.

Sample	T_g (K)	a	b	c
Cu–2 at. % Mn	16.0±0.5	3.3±0.2	0.15±0.1	0.67±0.06
Cu–5 at. % Mn	27.6	3.4	0.20	0.65
Cu–8 at. % Mn	37.7	3.6	0.19	0.65
Cu–10 at. % Mn	45.7	2.5	0.18	0.68
Cu-Mn_5Ge_5	23.5	1.8	0.18	0.65
Cu-Mn_5Ni_5	27.5	2.9	0.16	0.65
Ag-Mn 6.8	23.2	2.8	0.17	0.64
Cu–1 at. % Mn	11.5	2.7	0.14	0.60

III. EXPERIMENTAL TECHNIQUES

The samples were prepared by first forming an arc-melted button which was annealed under Ar at 700 °C for one day. The buttons were then rolled to foils 0.005 cm thick. Samples 0.4×6 cm^2 were vacuum annealed at 800 °C for one hour, and then air cooled. The ac susceptibility measurements were obtained primarily at 30 Hz in two types of apparatus. The sample was always moved between a pair of astatically wound coils which were located in the appropriate ac and dc magnetic fields. The dc field was varied from 0 to 7 kG, the ac field was at 30 Hz and typically $\cong$2 G. In one apparatus, the output signal from the coils was detected utilizing field-effect transistor (FET) electronics in a circuit incorporating electronic balancing signals as discussed below. In the other, the signal was measured utilizing superconducting coils and an associated superconducting quantum-interference device (SQUID) detector. The measurements of the dc magnetization were performed using a commercial SQUID magnetometer.[11]

The block diagram of the FET based instrument is shown in Fig. 4. An audio oscillator (1) provided the drive current to the primary coil (2). The oscillator output is also connected to a variable gain amplifier (5) and phase shifter (6). The output from the astatically wound pair of coils (3) is initially amplified (4) using a preamplifier, and then summed with the output of the phase shifter.

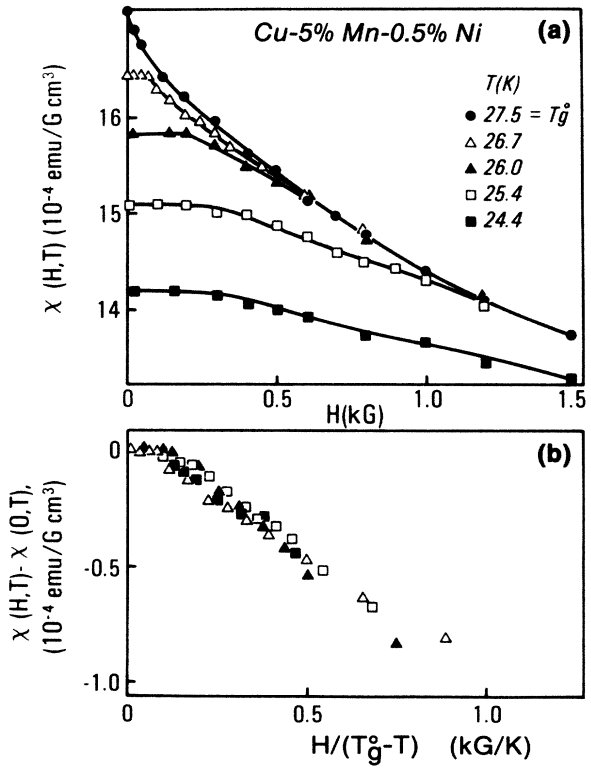

FIG. 3. The ac susceptibility data of Fig. 1 are replotted as a function of dc magnetic field for several values of temperature (all below T_g^0). In (b) we replot these data using the scaled axis as shown. We note that below T_g^0 the data satisfy a much simpler scaling relation than above T_g^0.

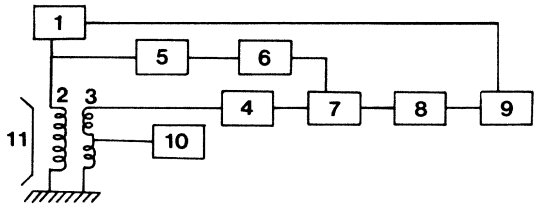

FIG. 4. Block diagram of the ac susceptibility apparatus utilizing FET electronics. (1) the audio frequency oscillator, (2) primary coil for ac field, (3) pair of astatically wound signal coils, (4) FET preamplifier, (5) variable gain amplifier, (6) phase shifter, (7) summing circuit, (8) narrow band filter, (9) lock-in amplifier, (10) DVM, (11) dc magnet. The sample is moved between the two signal coils as described in the text and illustrated in Fig. 5.

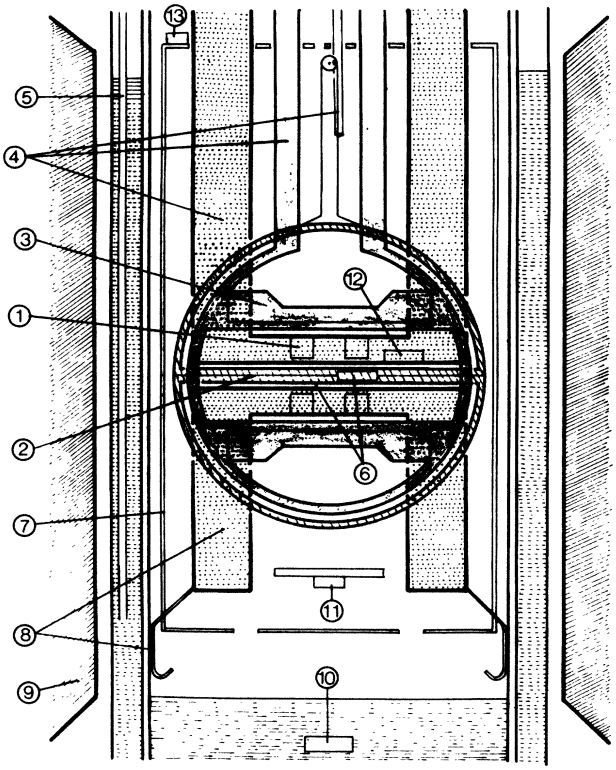

FIG. 5. Detailed scale drawing of the coils and sample arrangement: (1) the astatically wound pickup coils; (2) fine string used to push and/or pull the sample between the two coils of (1); (3) the primary ac coil, coaxial to (1); (4) Various parts of the support system to hold coils firmly in helium Dewar; (5) a fine gas tube in liquid-nitrogen jacket through which gas is blown to reduce bubbling; (6) sample holder containing rolled foil sample which slides in plastic tube; (7) thermal shield made of fine wires and epoxy to eliminate eddy current effects; (8) massive plastic holder with spring fingers to reduce vibration in helium Dewar; (9) external dc magnetic field, varian rotatable magnet with 4-in. gap; (10) heater in liquid helium to produce cooling vapor; (11) heater on thermal shield to regulate temperature; (12) cryogenic thermometer; (13) additional heater to maintain shield at desired uniform temperature.

The output of the summing circuit is additionally filtered (8) and then detected by a lock-in amplifier (9) referenced by the initial oscillator. A digital voltage meter (10) (DVM) is used for monitoring the coil voltages. The residual pickup signal due to imperfect balancing of the coils is further canceled by adjusting the variable attenuator and phase shifter to produce a minimum output at temperatures well above T_g. The phase of the lock-in is set to detect the in-phase signal component at the same temperature.

In Fig. 5 we present a scale diagram of the coil and sample arrangement. The sample (6) was moved back and forth between the two astatically wound coils (1) by a string (2) that was actuated outside the helium Dewar. The primary coil (3) was coaxial with the pickup coils. The assembly was contained within a constant temperature shield (7) made of fine copper wires and epoxy so as to eliminate eddy-current pickup. The temperature was sensed by resistive elements, and suitable heaters are placed on the shield and in the helium to allow setting and stabilizing of the temperature to between 1.5 and 77 K.

IV. INTERPRETATION

The striking consistency among the coefficients in Table I, over a broad range of samples, led us to suggest that the cusp line is a universal feature of metallic spin glasses, and we have endeavored to find a theoretical explanation for it. We note that the T dependence of the dc field suppression of χ in such differing materials as $La_{1-x}Gd_xAl_2$, (Ref. 5) and $Fe_{10}Ni_{70}P_{20}$, (Ref. 6) all also reveal a cusp line similar to that found for Cu-Mn as in Figs. 1, 8, and 9.

We first observe that the very large suppression of the dc susceptibility by a weak dc magnetic field[2] is greatly underestimated by current spin-glass theories if one assumes individual spin moments. Experimentally, one finds for Cu-Mn $\Delta\chi/\chi = 17\%/\text{kG}$ of applied dc field. In an attempt to fit their dc magnetization data at $H = 220$ G to expressions developed by Toulouse and Gabay,[12] Chamberlain *et al.*[7] concluded that the field had to be rescaled by a factor of 28. We interpret this discrepancy as a fundamental limitation on describing the magnetization near T_g^0 by the response of individual spins. We regard the suppression as a consequence of a much larger effective spin size entity, which we term a spin cluster.

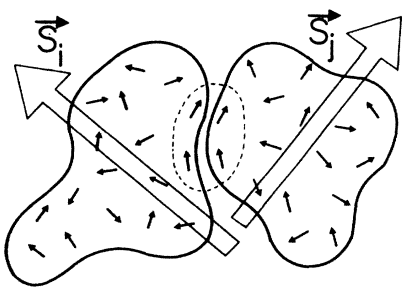

FIG. 6. The intracluster spin exchange gives rise to a net spin $\mathbf{S}_i$ and $\mathbf{S}_j$, respectively. The intercluster spin exchange J_{ij} is dominated by the nearest spins as indicated in the figure, resulting in the equilibrium configuration having the random angle θ_{ij}.

Once we admit to spin clusters, one may examine their response to applied ac fields. In what follows, we develop a model in which individual clusters, with random initial equilibrium moment directions and a rotationally invariant exchange interaction, attempt to rotate in response to an applied ac field. We find that the dynamical description of the local field leads to a new rotational correlation length which we evaluate using model parameters fit to the data of the dc field suppression of the ac and dc χ. We identify the divergence of the rotational correlation length with the observed cusp line displayed in Fig. 1 and parametrized in Table I.

V. THEORY OF A CLUSTER SPIN-GLASS MODEL LEADING TO A NEW LOCAL-FIELD CORRELATION LENGTH

We consider the individual spins $\mathbf{s}_j$ as spontaneously forming clusters of net spin $\mathbf{S}_i$ with an average spin size S, which is a function of the external dc magnetic field H, and the temperature T. For T well above the spin-glass transition temperature, $T_g(H)$, the clusters rotate relatively independently in response to a low-frequency applied ac magnetic field, and hence the system exhibits a parallel ac susceptibility χ which is close to a Curie law. At T near $T_g(H)$, we will show that the theory predicts the development of a long-range rotational correlation length for the local field $\mathbf{H}_i$, which is felt by each net cluster spin, $\mathbf{S}_i$. This dynamical local-field correlation in turn manifests itself in a special long-range behavior characterizing the rotational properties of the clusters. We postulate that at the temperature where the local-field correlation length diverges, we should expect an anomaly in the measured χ, depending on the frequency. Using cluster parameters fitted to our data above $T_g(H)$, we are able to predict the divergence temperature and find qualitative agreement with a new cusplike feature observed in our experiments.

At any given H and T, the ith cluster is composed of randomly oriented n_i individual spins $\mathbf{S}_i = \sum^n \mathbf{s}_j$. The average cluster spin $S(H,T) = \sum^N |\mathbf{S}_i| / N$, where N is the total number of clusters. We define the average number of spins per cluster, n, via $S = \sqrt{n}\,|s_j|$ and the total number of spins as N^0. In what follows, we take $|\mathbf{s}_j|$ to be unity, and thus $N^0 = nN = S^2N$. S will be sufficiently large such that we may regard the spin as classical in defining the thermally averaged magnetic moment of the ith cluster as

$$\mathbf{M}_i = [(\mathbf{H}+\mathbf{H}_i)/|\mathbf{H}+\mathbf{H}_i|]SL(S|\mathbf{H}+\mathbf{H}_i|/T)\,, \quad (1)$$

where T is in units of T_g^0, H and H_i in units of $k_B T_g^0/g\mu_B$. M is in units of $g\mu_B$ and L is the Langevin function.

Before we present an expression for the total energy we must explain the meaning of a special operator, $\tilde{R}_{ij}$. We take the interaction energy of any two clusters to be a function of their relative orientation and an exchange parameter J_{ij}. However, in contrast to the usual theories, we postulate that the minimum energy orientation of any two interacting spin clusters, $\mathbf{S}_i$ and $\mathbf{S}_j$, may be *at any an-*

gle independent of J_{ij}. Since this is a quite different description than the one of the models frequently employed, we digress to present a simplified picture of how this might come about. In Fig. 6 we schematically represent the two clusters in their minimum energy configuration. Each of the clusters is, in turn, comprised of many individual spins which interact via some exchange interaction with their counterparts in the other cluster. If the energy between the individual spins nearest each other dominates the total cluster-cluster interaction energy, and their local exchange constant was such as to require parallel spins, the equilibrium configuration would be as shown. The relative angle θ_{ij} between $\mathbf{S}_i,\mathbf{S}_j$ is described by the operator $\tilde{R}_{ij}(\theta_{ij})$ and the two-cluster contribution to the energy is given by $E_{ij}=J_{ij}\mathbf{S}_i\cdot\tilde{R}_{ij}\mathbf{S}_j$.

Because the anisotropy energy for Cu-Mn is much smaller than the Ruderman-Kittel-Kasuya-Yosida (RKKY) energy [at 1 at.% Mn, E(anisotropy)/E(RKKY)=0.003],[13] we do not incorporate anisotropy in our initial formulation, and hence take our model Hamiltonian as *rotationally invariant.* For simplicity, in the development of the subsequent theory, we shall restrict ourselves to a two-dimensional spin system, hence all rotations are about an axis perpendicular to the plane. In this case, $\tilde{R}_{ij}(\theta_{ij})$ is simply the rotation operator which rotates $\mathbf{S}_j$ toward $\mathbf{S}_i$ by the angle θ_{ij} and E_{ij} is rotationally invariant. We may now write the total energy of the cluster spin system as

$$E=\sum_{i,j(i>j)} J_{ij}\mathbf{S}_i\cdot\tilde{R}_{ij}\mathbf{S}_j-\sum_i \mathbf{H}\cdot\mathbf{S}_i\ , \tag{2}$$

where we take the distribution of the equilibrium θ_{ij} to be uniformly random for all angles, and the J_{ij} to be represented by a random Gaussian distribution $P(J_{ij})$ of variance $J(H,T)$. We make the further assumption that the spin clusters will only interact appreciably with nearest neighbors, whose number we characterize by an average neighborhood number, Z. (We visualize $Z\sim 10$.) Thus in what follows, when we wish to determine the average local field at a given cluster, we shall only regard such sums as being over a number Z. We take the local field at site i to be given by a mean-field expression including the leading term in the Onsager local-field correction:[14]

$$\mathbf{H}_i=\sum_{j=1}^{Z} J_{ij}\tilde{R}_{ij}\mathbf{M}_j-J^2\sum_{j=1}^{Z}(\tilde{R}_{ji}\mathbf{M}_i\cdot\partial/\partial\mathbf{H}_j)\tilde{R}_{ij}\mathbf{M}_j\ , \tag{3}$$

where $\partial/\partial\mathbf{H}=\nabla_{\mathbf{H}}$.

We now define a particular averaging procedure for any thermally averaged variable, such as the $\mathbf{M}_i$ or $\mathbf{H}_i$, given by

$$\{Q\}\equiv\int P(J_{ij})\prod_{i,j}dJ_{ij}\int\prod_{i,j}d\Omega_{ij}Q \tag{4}$$

where $d\Omega_{ij}$ is the solid angle element which enters because of the random rotational angle of the $\tilde{R}_{ij}$ and $\prod_{ij}d\Omega_{ij}$ is the product of all $d\Omega_{ij}$'s. From this definition one may show that $\{J_{ij}Q\}=J^2\{\partial Q/\partial J_{ij}\}$ and that to first approximation $\partial\mathbf{H}_j/\partial J_{ij}\sim\tilde{R}_{ji}\mathbf{M}_i$. (See Appendix A 1 b.) Using Eq. (3) with these two equations, we can further show that $\{\mathbf{H}_i\}=0$ (see Appendix A 2 a), and that again to a first approximation: (see Appendix A 2 b and 2 c)

$$\{\mathbf{H}_i\cdot\mathbf{H}_i\}=J^2\sum_{j=1}^{Z}\{\mathbf{M}_j\cdot\mathbf{M}_j\}$$

and (5)

$$\{\mathbf{H}_i\times d\mathbf{H}_i\}=J^2\sum_{j=1}^{Z}\{\mathbf{M}_j\times d\mathbf{M}_j\}$$

where $d\mathbf{H}_i$ is to be regarded as a change of the local field for the ith cluster, in the time interval and caused, for example, by an applied perturbation at some other cluster away from site i. Similarly, $d\mathbf{M}_i$ is the associated change in the thermally averaged moment of the cluster.

We now seek to write an alternate expression for (5) using the probability distribution for $\mathbf{H}_i$, $P(\mathbf{H}_i)$. We take $P(\mathbf{H}_i)$ to be isotropic (see Appendix B) and to be characterized by an appropriate distribution with variance $h(T,H)$. Thus we convert the $\{Q\}$ averages over $P(J_{ij})$ to $\langle Q\rangle$ averages over $P(\mathbf{H}_i)$. This procedure would require a specific representation for the $P(\mathbf{H}_i)$ to be exact, but we assume that a suitable approximation is an isotropic Gaussian distribution (see Appendix C) such that $h^2=\langle\mathbf{H}_i\cdot\mathbf{H}_i\rangle$, where

$$\langle Q\rangle=\int QP(\mathbf{H}_i)\prod_i d^3H_i\ . \tag{6}$$

Assuming the mean-field condition: $\langle\mathbf{M}_i\cdot\mathbf{M}_i\rangle=\langle\mathbf{M}_j\cdot\mathbf{M}_j\rangle$, we find

$$h^2=ZJ^2\langle\mathbf{M}_i\cdot\mathbf{M}_i\rangle\ . \tag{7}$$

If $\mathbf{H}_j$ is changed to $\mathbf{H}_j+d\mathbf{H}_j$ by some perturbation of the system, we obtain $d\mathbf{M}_j$ from Eq. (1) and form

$$\mathbf{M}_j\times d\mathbf{M}_j=(S^4/T^2)L_0^2(S\mid\mathbf{H}+\mathbf{H}_j\mid/T)\cdot(\mathbf{H}+\mathbf{H}_j)\times d\mathbf{H}_j$$

where $L_0(x)=1/xL(x)$. Assuming $d\mathbf{H}_j$ is isotropically random, we have

$$\langle\mathbf{M}_j\times d\mathbf{M}_j\rangle\approx(S^4/T^2)\langle L_0^2\rangle\langle\mathbf{H}_j\times d\mathbf{H}_j\rangle\ . \tag{8}$$

If we define $\mathbf{F}_i=\langle\mathbf{H}_i\times d\mathbf{H}_i\rangle$, which we take as the simplest dynamical quantity to measure rotational changes of $\mathbf{H}_i$, and combine Eq. (8) with Eq. (5), we find the important equation describing the propagation of a local-field rotational disturbance,

$$\mathbf{F}_i=(J^2S^4/T^2)\langle L_0^2\rangle\sum^{Z}\mathbf{F}_j\ . \tag{9}$$

We recognize Eq. (9) as a difference equation being convertible to the form: $(\nabla^2-k^2)\mathbf{F}(r)=\mathbf{0}$, where $k^2=6/l^2(T^2/ZJ^2S^4\langle L_0^2\rangle-1)$ and l is the mean distance between clusters. We identify the condition $k=0$ as when the local-field correlation length becomes infinite, corresponding to

$$T_g^2=ZJ^2S^4\langle L_0^2\rangle\Big|_{T=T_g}\ . \tag{10}$$

In Appendix D we show that the instability associated with the quantity $\mathbf{H}_i\times d\mathbf{H}_i$ leading to the transition temperature relation of Eq. (10) always occurs at a higher

temperature than that associated with the instability associated with the quantity $\mathbf{H}_i \cdot d\mathbf{H}_i$. We determine the value of T_g corresponding to a given value of H by a self-consistent solution of Eq. (10) with the following computational sequence. We first determine the two parameters of the model, $S(H,T)$ and $K_0 = ZJ^2S^4$, by fitting the differential dc magnetization, $\Delta\mathbf{M}/\Delta\mathbf{H} \equiv \chi_d$ to the data.[15] We obtain a theoretical expression for χ_d by differentiating Eq. (1), which, when normalized to unity at $H=0$ and $T=1$, is

$$\chi_d = (3N/N_0) d\langle \mathbf{M}_i \cdot \hat{Z} \rangle / dH \ . \tag{11}$$

Equation (11) in conjunction with Eq. (7) is equivalent to the S-K[16] solution, which we note is very close to the χ_d of the Parisi solution[17] over the temperature range covered. We assume that χ_d is equal to our measured ac χ for all temperatures above T_g^0, and that it remains constant at the plateau value for all $T < T_g^0$. (The latter corresponding to the observation that the dc magnetization is nearly independent of T below T_g^0.) We note that χ_d is independent of S at $H=0$, and hence we can evaluate $K_0(T,0)$. We find that K_0 is essentially constant with temperature, and hence we assume that it will be even less dependent on magnetic field. Thus, we take K_0 to be independent of H, and equal to $K_0(T_g^0)$ for all $T > T_g^0$ where the normalization makes $K_0 = 9$. Below T_g^0, K_0 has a mild temperature dependence which is fit to the data. For finite H we determine the value of S which results in a self-consistent fit to the χ data via Eqs. (7) and (11). In Fig. 7 we present the values of $2S$ as a function of H for several T. Using the values of S recovered from the data fitting procedure just described, we may determine values of T_g as a function of H from a self-consistent solution of Eq. (10).

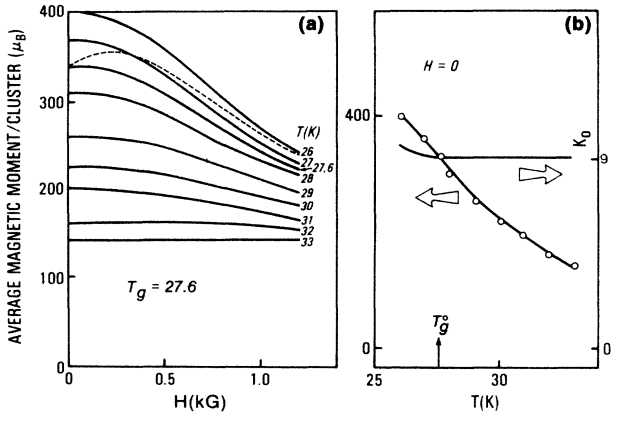

FIG. 7. In (a) we present the values of average magnetic moment ($2S$) per cluster as deduced via the fitting to the data as discussed in the text. We obtain very nearly the same values for either case (a) or case (b) of the $P(H_i)$ distribution used to obtain curves 2 and 3, respectively, in Fig. 8. The $P(H_i)$ of cases (a) and (b) are described in the first paragraph of Sec. V. In (b) the open circles represent values of $2S$ as a function of temperature when the dc field is equal to zero. The solid line represents values of K_0 for the $P(H_i)$ of case (b). For case (a), K_0 is nearly independent of temperature even below T_g.

VI. COMPARISON OF THEORY AND EXPERIMENT

In Fig. 8 we compare our data of Fig. 1 with values of $T_g(H)$ predicted via the procedure just described, for two forms of the $P(H_i)$.[18] We find qualitative agreement with case (a)

$$P(H_i) \propto H_i^2 \exp(-3H_i^2/2h^2) dH_i d\Omega$$

[curve (2)], and excellent agreement for the modified distribution; case (b):

$$P(H_i) \propto \exp(-H_i^2/2h^2) dH_i d\Omega$$

[curve (3)]. In Fig. 9 we present a comparison between data for another sample concentration, over an extended H range with the predictions utilizing the case (b) $P(H_i)$. Again, we find very good agreement.

In Fig. 8 we also present values of $T_g(H)$ determined from expressions for the de Almeida–Thouless[19] (AT) and Gabay-Toulouse[12] (GT) formulations for the phase transition. The $\Delta\chi$ and ΔT relations that are used are for the AT formulation (see Ref. 20)

$$\Delta T = [(m+1)(m+2)/8]^{1/3} H^{2/3} \ ,$$
$$M/H = 1 - \tfrac{3}{4}[4/m+2]^{1/3} H^{4/3} \tag{12}$$

(see Refs. 7 and 21), and for the GT formulation (see Refs. 20 and 21),

$$\Delta T = (m^2+4m+2)H^2/4(m+2)^2 \ ,$$
$$M/H = 1 - H/\sqrt{2} \tag{13}$$

(see Refs. 7 and 22) for $m=3$, and $\chi = dM/dH$, and

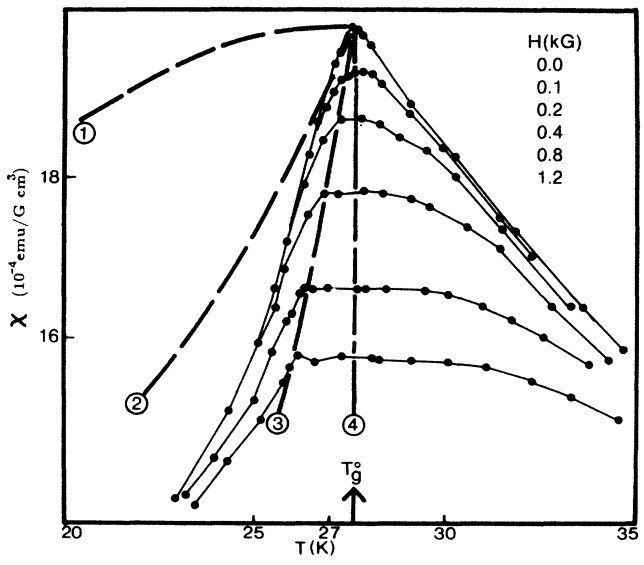

FIG. 8. A comparison of the experimental data of Fig. 1 with several theoretical expressions discussed in the text. Curve 1, the AT transition as represented by Eq. (14). Curve 2, determined via the theory described in the text and using the $P(H_i)$ of case (a). Curve 3, similar to curve 2 except utilizing the $P(H_i)$ of case (b). Curve 4, the GT transition as represented by Eq. (15). The $P(H_i)$ of cases (a) and (b) are presented in the first paragraph of Sec. V.

$\Delta\chi = 1 - \chi$ we obtain for the AT formulation,

$$\Delta\chi = (\tfrac{7}{4})(\tfrac{4}{5})^{1/3}(\tfrac{8}{20})^{2/3}\Delta T^2 , \quad (14)$$

and for the GT formulation,

$$\Delta\chi = \sqrt{2}(\tfrac{100}{23})^{1/2}\Delta T^{1/2} . \quad (15)$$

The curves obtained using Eqs. (14) and (15) are displayed on Fig. 8, labeled 1 and 4, respectively. We see that both the AT and GT transition relations are clearly inconsistent with the experimental cusp line. The same observation applies to the data presented in Fig. 9 for a Cu—1 at. % Mn sample.

We have previously mentioned the failure of the GT formulation to account for the magnitude of the very large suppression of the ac or dc susceptibility by weak applied dc magnetic fields. This same observation applies to the AT formulation as well, as long as the moments are taken to be those corresponding to single atomic spins. We regard that as a serious limitation to the applicability of these formulations, and as noted, this observation provided the initial impetus to incorporate a cluster model from the outset. We wish to further point out, however, that the relations of Eqs. (14) and (15) are independent of the observed spin value and hence even with an adjustment of the spin moment, neither formulation appears likely to be associated with our observed cusp line feature.

In Fig. 10, we plot the reduced field, $H_r^{2/3}$ versus $\Delta T/T_g^0$, for a Cu—1 at. % Mn sample, over an extended field range up to $H = 7$ kG. Here, H_r is in units of $k_B T_g^0/g\mu_B$. These conditions were chosen so as to allow comparison with the recent torque data reported by de Courtenay *et al.*,[23] who compared their deduced feature near T_g with the behavior predicted by Kotliar and Sompolinsky.[24] The material presented in Fig. 10 may be summarized as follows.

(1) The data have a $H^{2/3}$ dependence to quite high fields, and correspondingly large shifts of T_g.

(2) The results of our rotational correlation theory utilizing the case (b) $P(H_i)$ (open circles) are in excellent agreement with our data (crosses).

(3) The GT relation of Eq. (13) is not plotted in Fig. 10 because it would simply lie along the vertical axis for the range of fields covered. Thus, we confirm the interpretation of Figs. 8 and 9 that the GT relation cannot be identified with our data.

(4) While the AT criteria agrees with the observed $H^{2/3}$ dependence, (although the shape is off by a factor $\equiv 2$), the $\Delta\chi$-ΔT relation is quantitatively so far off (see Fig. 8), that it cannot likely be identified with the data.

(5) The transition feature reported by de Courtenay *et al.*[23] (open squares) would seem to correspond to an entirely different phenomena.

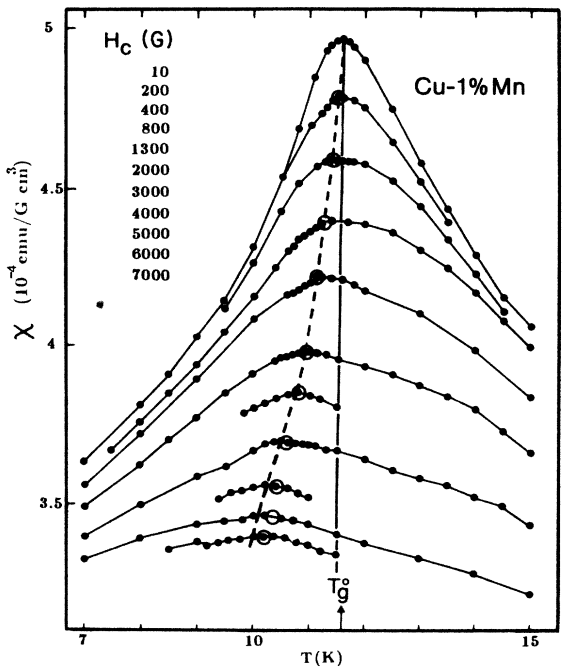

FIG. 9. The parallel ac susceptibility of a 1 at. % Cu-Mn foil as a function of temperature for values of applied field up to 7 kG. The dashed curve represents the locus of the cusp line which exhibits the curvature as shown for higher magnetic fields. The open circles are points calculated using the $P(H_i)$ of case (b), following the data analysis procedure as described in the text. The solid line is for the GT expression given in Eq. (15).

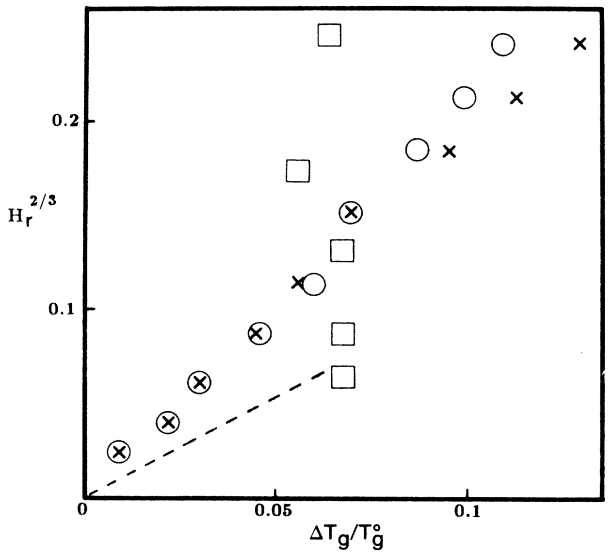

FIG. 10. The reduced field, H_r, to the $\frac{2}{3}$ power versus $\Delta T_g/T_g^0$ as determined from the data of Fig. 9. The crosses ($\times$) represent the data of the cusp line. The circles are points calculated using the $P(H_i)$ of case (b). Were the GT relation of Eq. (13) plotted for the scale of Fig. 10, it would be essentially a vertical line from the origin. The dashed curve represents the AT expression of Eq. (14), but with S taken as 1 rather than being adjusted so as to insure agreement with the large suppression of the dc susceptibility in the magnetic field. (Were the correct S values used, the dashed line would be nearly horizontal.) The squares are taken from Fig. 2 of Ref. 23, where they identify a transition feature associated with zero torque on their spin-glass sample. It would appear that the torque feature measures an entirely different property than that associated with the cusp line of Fig. 1 or 8.

VII. CONCLUSION

We present extended measurements of the temperature and dc magnetic field dependence of the parallel ac susceptibility,[4] for the Cu-Mn spin-glass system. We find that there is a large suppression of χ for weak magnetic fields, and that for modest field values as one lowers the temperature below T_g^0, χ becomes almost independent of temperature before exhibiting an abrupt change of slope at a well-defined temperature. We have attempted to identify the locus of this observed feature with the well-known de Almeida–Thouless[19] or Gabay-Toulouse[12] transitions and find that they are in clear disagreement. This disagreement has led us to seek an alternate formulation of the problem, and we have developed a phenomenological model which appears to have considerable success in predicting the observed transition feature, using model parameters obtained by a parametrization of the ac and dc susceptibility data.

We interpret the very large suppression of the ac and dc susceptibilities by weak applied magnetic fields as being indicative of cooperative spin behavior, which we term a spin cluster. We find that a theoretical examination of the response of these exchange coupled clusters to an external ac magnetic field leads to the prediction that there is a local-field rotational correlation length in spin glasses. We identify the divergence of this correlation length as occurring at the T and H for which we observe a new cusp feature in the temperature dependence of the ac susceptibility measured in modest applied dc magnetic fields. The new feature we have observed experimentally appears in so many samples, and with striking similarity (as displayed in Table I), that we regard it as an inherent property of metallic spin-glass systems.

It is clear that there are many simplifications incorporated in our model and analysis. Nonetheless, we believe that the basic assumptions of the model have merit, and warrant further study. We would expect that there may be other indications of the local-field rotational correlation length we have developed.

We cannot help but note the remarkable agreement between our data and the predictions of our theory utilizing the case (b) local-field probability distribution function. The formation of clusters likely depends on both the physical distribution of the moments and the consequent interactions. Once the clusters are formed, they, in turn, determine the appropriate $P(J_{ij})$ distribution. We suggest that it would be of value to ascertain the particular $P(H_i)$ distribution to which a given $P(J_{ij})$ corresponds. In principle, it should be possible to determine one distribution function given the other, and while this is a worthwhile effort for its own sake, there may be important physical insight in terms of interpreting the one that appears to fit the data so well.

We have confirmed that the transition line is qualitatively the same for frequencies of $\sim 10^{-3}$ to 700 Hz. Therefore, we believe that the dynamical correlation persists for the corresponding time scale. It would be of great interest to determine the nature of the dynamical correlation to much longer and shorter time scales via future experiments.

We find that our data are well represented by the scaling relations indicated in Figs. 3 and 4 for temperature above and below T_g, respectively. The values of the critical exponents deduced are compared with those of other experiments in Table II. We note that our data below T_g were taken via two temperature field sequences, as explained in Sec. II, and thus we feel that they are representative of a meaningful equilibrium condition.

ACKNOWLEDGMENTS

We gratefully thank Professor D. Fredkin, J. Hertz, and Dr. G. Kotliar for their extensive and patient help with our theoretical analysis. We thank Professor R. Orbach, J. Mydosh, M. Salamon, and Dr. R. V. Chamberlain, and Dr. A. P. Malozemoff for helpful conversations. This work was supported by National Science Foundation under Grant No. DMR 83 12450.

APPENDIX A

In this appendix we present a proof for various relations utilized in our development of the theoretical model in Sec. V. In Part 1 we develop several useful general relations which are then used to establish more specific relations in Part 2.

1. General relations

The general relations are listed as follows.

TABLE II. Critical exponents (Mn concentrations in at. %). Listed are the critical exponents of several samples. (The definition of δ' and γ' are given in the text.)

	(a) Above T_g				
	Ref. 4	Ref. 13	Ref. 25	Ref. 26	This work
	Ag-Mn(10.6)	Gd-Al	Cu-Mn(1)	Ag-Mn	Cu-Mn(5)
δ	2.0	5.7±0.2	5.7±0.5	3.0±0.2	3.0±0.8
γ	1.5±0.5	2.7±1.0	3.3±0.05	2.2±0.1	1.85±0.5

	(b) Below T_g
	$Cu\text{-}Mn_5Ni_{0.5}$ [this work (χ_{ac})]
δ'	2.0
γ'	1.0

a. $\{J_{ij}\times Q\}$

We have

$$\{J_{ij}\times Q\}=J^2\{\partial/\partial J_{ij}Q\}\ , \tag{A1}$$

where Q is any system variable, and the $\{\ \}$ represent a particular averaging process defined by Eq. (4). We note this relation holds because we have taken a Gaussian distribution for $P(J_{ij})$.

b. $\partial\mathbf{H}_j/\partial J_{ij}$

We have

$$\partial\mathbf{H}_j/\partial J_{ij}\equiv\tilde{R}_{ji}\mathbf{M}_i\ . \tag{A2}$$

This relation is not exact because we drop the J_{ij} derivative of the Onsager correlation term to the internal field [see Eq. (3)]. We note that the omitted term is of the form $J^2\sum(\tilde{R}_{ji}\mathbf{M}_i\cdot\partial/\partial\mathbf{H}_j)\tilde{R}_{ij}\mathbf{M}_j$, and therefore of higher order of J than the leading term.

c. Internal field equation

The internal field equation, Eq. (3), can be rewritten as

$$\mathbf{H}_i\equiv\sum_j[J_{ij}-J^2(\partial/\partial J_{ij})]\tilde{R}_{ij}\mathbf{M}_j \tag{A3}$$

by the use of (A2) as follows. From Eq. (3) we have

$$\mathbf{H}_i=\sum_j J_{ij}\tilde{R}_{ij}\mathbf{M}_j-J^2\sum_j[\tilde{R}_{ji}\mathbf{M}_j(\partial/\partial\mathbf{H}_j)]\tilde{R}_{ij}\mathbf{M}_j\ .$$

We replace $\tilde{R}_{ji}\mathbf{M}_i$ in the second term by $\partial\mathbf{H}_j/\partial J_{ij}$ [using (A2)]; and note that

$$(\partial\mathbf{H}_j/\partial J_{ij})(\partial/\partial\mathbf{H}_j)\tilde{R}_{ij}\mathbf{M}_j=(\partial/\partial J_{ij})\tilde{R}_{ij}\mathbf{M}_j$$

because the only explicit variable dependence in $\mathbf{M}_j$ is on $\mathbf{H}_j$.

d. $\{\mathbf{C}\times H_i\}$

We evaluate the quantity $\{\mathbf{C}\times\mathbf{H}_i\}$ or $\{\mathbf{C}\cdot\mathbf{H}_i\}$ where $\mathbf{C}$ is any vector quantity in an identical manner; and hence we only present the procedure for one:

$$\{\mathbf{C}\times\mathbf{H}_i\}=J^2\sum_j\{(\partial/\partial J_{ij}\mathbf{C})\times\tilde{R}_{ij}\mathbf{M}_j\}\ . \tag{A4}$$

Proof:

$$\{\mathbf{C}\times\mathbf{H}_i\}=\{\mathbf{C}\times\sum_j(J_{ij}-J^2[\partial/\partial J_{ij}])\tilde{R}_{ij}\mathbf{M}_j\}\ ,$$

using (A3). To evaluate the right-hand side of (A4), we identify the quantity $\mathbf{C}\times\tilde{R}_{ij}\mathbf{M}_j$ as a Q factor in the sense of (A1) and making use of (A1) we may express it as

$$\{\mathbf{C}\times\mathbf{H}_i\}=J^2\sum_j\{(\partial\mathbf{C}/\partial J_{ij})\times\tilde{R}_{ij}\mathbf{M}_j+\mathbf{C}\times[\partial/\partial J_{ij}(\tilde{R}_{ij}\mathbf{M}_j)]-\mathbf{C}\times[\partial(\tilde{R}_{ij}\mathbf{M}_j)/\partial J_{ij}]\}\ .$$

The last two terms cancel, thereby proving (A4).

e. Scalar quantity

For any scalar quantity, a, we find

$$\{a\mathbf{H}_i\}=J^2\sum_j\{[(\partial/\partial J_{ij})a]\tilde{R}_{ij}\mathbf{M}_j\} \tag{A5}$$

by the same argument as in (4).

2. Specific relations

Having prepared the relations (A1) to (A5) in part 1, we now establish some specific results.

a. $\{\mathbf{H}_i\}$

We have,

$$\{\mathbf{H}_i\}=0\ . \tag{A6}$$

This follows by letting $a=1$ in (A5).

b. $\{\mathbf{H}_i\times d\mathbf{H}_i\}$

Here,

$$\{\mathbf{H}_i\times d\mathbf{H}_i\}=J^2\sum_j\{\mathbf{M}_j\times d\mathbf{M}_j\}\ . \tag{A7}$$

Proof: Let $\mathbf{H}_i'\equiv\mathbf{H}_i+d\mathbf{H}_i$ and $\mathbf{M}_j'\equiv\mathbf{M}_j+d\mathbf{M}_j$. Hence $\{\mathbf{H}_i\times d\mathbf{H}_i\}=-\{\mathbf{H}_i'\times\mathbf{H}_i\}$.

We regard $\mathbf{H}_i$ as the quantity $\mathbf{C}$ in (A4) and it follows that

$$\{\mathbf{H}_i'\times\mathbf{H}_i\}=J^2\sum_j\{[(\partial/\partial J_{ij})\mathbf{H}_i']\times\tilde{R}_{ij}\mathbf{M}_j\}$$
$$=J^2\sum_j\{\tilde{R}_{ij}\mathbf{M}_j'\times\tilde{R}_{ij}\mathbf{M}_j\},\ \text{[using (A2)]}\ .$$

Since the vectors product is rotationally invariant in two dimensions, we then have

$$=J^2\sum_j\{\mathbf{M}_j'\times\mathbf{M}_j\}=J^2\sum_j\{d\mathbf{M}_j\times\mathbf{M}_j\}\ ,$$

thereby verifying (A7).

c. $\{\mathbf{H}_i\cdot\mathbf{H}_i\}$

Here,

$$\{\mathbf{H}_i\cdot\mathbf{H}_i\}=J^2\sum_j\{\mathbf{M}_j\cdot\mathbf{M}_j\}\ . \tag{A8}$$

This is proven by analogy to (b) above, and recalling that (A4) held for either cross or dot product.

APPENDIX B

Here, we prove that if $P(J_{ij})$ is a Gaussian distribution and R_{ij} is a random angle rotation operator in two dimensions, as assumed in Sec. V, then the internal field probability distribution $P(\mathbf{H}_i)$ is isotopic.

Proof: We observe that if $\{\mathbf{H}_i\}=0$, and $[(H_i^x)^2]=[(H_i^y)^2]$ where H_i^x is the x component of $\mathbf{H}_i$, etc., then $P(H_i)$ is isotropic. Now $\{\mathbf{H}_i\}=0$ by (A6); and if we identify H_i^x as the "a" factor in (A5), then we have

$$\{(H_i^x)^2\} = J^2 \sum_j [(\partial/\partial J_{ij}) H_i^x][(\tilde{R}_{ij}\mathbf{M}_j)^x]$$
$$= J^2 \sum_j \{(\tilde{R}_{ij}\mathbf{M}_j)^x (\tilde{R}_{ij}\mathbf{M}_j)^x\} \quad \text{[using (A2)]}$$
$$= J^2 \sum_j \{[(\tilde{R}_{ij}\mathbf{M}_j)^x]^2\} .$$

Since $\tilde{R}_{ij}$ is a uniformly randomly distributed rotation operator, this last quantity is independent of any particular component direction, and hence is the same value for the x or y component. Thus $\{(H_i^x)^2\} = \{(H_i^y)^2\}$, as was to be shown.

APPENDIX C

We prove that if $P(J_{ij})$ is a Gaussian random distribution, then $P(\mathbf{H}_j)$ is also a Gaussian distribution:

$$\{(H_i^x)^{2\eta}\} = \{(H_i^x)^{2\eta-1}(\mathbf{H}_i)^x\}$$
$$= J^2 \sum_i \{[\partial/\partial J_{ij}(H_i^x)^{2\eta-1}](\tilde{R}_{ij}\mathbf{M}_j)^x\} \quad \text{[from (A5)]}$$
$$= (2\eta-1)J^2 \sum_j \{(H_i^x)^{2\eta-2}[(\partial \mathbf{H}_i)/\partial J_{ij}]^x (\tilde{R}_{ij}\mathbf{M}_j)^x\}$$
$$= (2\eta-1)J^2 \sum_j \{(H_i^x)^{2\eta-2}[(\tilde{R}_{ij}\mathbf{M}_j)^x]^2\} \quad \text{[using (A2)]}$$
$$\cong (2\eta-1)J^2\{(H_i^x)^{2\eta-2}\} \left\{ \sum_j [(\tilde{R}_{ij}\mathbf{M}_j)^x]^2 \right\} ,$$

where we have replaced the $\{\ \}$ expression of the preceding line by a product of $\{\ \}\cdot\{\ \}$ factors. This last relation is characteristic of a Gaussian distribution with the variance approximately equal to $\{J^2 \sum_j [(\tilde{R}_{ij}\mathbf{M}_j)^x]^2\}$, as in Appendix B.

APPENDIX D

We wish to show that the instability associated with the quantity $\mathbf{H}_i \times d\mathbf{H}_i$ leading to the transition temperature relation of Eq. (10) always occurs at a higher temperature than that associated with the instability associated with the quantity $\mathbf{H}_i \cdot d\mathbf{H}_i$ (i.e., analogous to the AT transition).[18]

From Eq. (1) and using $L_0(x) \equiv L(x)/x$, we have

$$\mathbf{M}_i = (\mathbf{H}+\mathbf{H}_i)(S^2/T) L_0(S\,|\,\mathbf{H}+\mathbf{H}_i\,|\,/T) ,$$

where

$$d\mathbf{M}_i = d\mathbf{H}_i \cdot S^2 L_0/T + (\mathbf{H}+\mathbf{H}_i)(S^2/T) L_0' \cdot S/T(\mathbf{H}+\mathbf{H}_i)/|\,\mathbf{H}+\mathbf{H}_i\,| \cdot d\mathbf{H}_i ,$$

where L_0' means $(d/dx)L_0(x)$. Using the $\langle\ \rangle$ averaging process defined by Eq. (6), we have

$$\langle \mathbf{M}_i \cdot d\mathbf{M}_i \rangle = S^4 \langle L_0^2 \rangle / T^2 \cdot \langle \mathbf{H} \cdot d\mathbf{H}_i + \mathbf{H}_i \cdot d\mathbf{H}_i \rangle$$
$$+ S^5 \langle L_0 L_0'/T^3\,|\,\mathbf{H}+\mathbf{H}_i\,|\,(\mathbf{H}+\mathbf{H}_i)\cdot d\mathbf{H}_i \rangle .$$

We note that $\langle \mathbf{H} \cdot d\mathbf{H}_i \rangle = 0$ and that the second term on the right-hand side of the expression may be written as

$$\cong (S^5 \langle L_0 L_0'\rangle/T^3)\langle\,|\,\mathbf{H}+\mathbf{H}_i\,|\,\rangle \langle (\mathbf{H}+\mathbf{H}_i)\cdot d\mathbf{H}_i \rangle$$
$$= (S^5 \langle L_0 L_0' \rangle)/T^3 \langle\,|\,\mathbf{H}+\mathbf{H}_i\,|\,\rangle \langle \mathbf{H}_i \cdot d\mathbf{H}_i \rangle ,$$

which is equal to a negative number $x\langle \mathbf{H}_i \cdot d\mathbf{H}_i \rangle$ because L_0' is always negative. Hence

$$\langle \mathbf{M}_i \cdot d\mathbf{M}_i \rangle = (S^4 \langle L_0^2 \rangle)/T^2 (1 + \text{ negative number})$$
$$\times \langle \mathbf{H}_i \cdot d\mathbf{H}_i \rangle .$$

Thus, in analogy with the $\langle \mathbf{M}_i \times d\mathbf{M}_i \rangle$ instability, the $\langle \mathbf{M}_i \cdot d\mathbf{M}_i \rangle$ instability occurs when

$$(ZJ^2 S^4 \langle L_0^2 \rangle)/T_g'^2 (1 + \text{ negative number}) = 1 ,$$

whereas $\langle \mathbf{M}_i \times d\mathbf{M}_i \rangle$ instability occurs when $(ZJ^2 S^4 \langle L_0^2 \rangle)/T_g^2 = 1$, therefore $T_g' < T_g$ as was to be shown.

[1]See the review article by K. H. Fischer, Phys. Status Solidi B **130**, 13 (1985).

[2]P. Monod and H. Bouchiat, in *Disordered Systems and Localization*, Vol. 149 of *Lecture Notes in Physics*, edited by C. Castellani, C. Di Castro, and L. Peliti (Springer-Verlag, Berlin, 1981).

[3]V. Cannella and J. Mydosh, Phys. Rev. B **6**, 4220 (1972).

[4]J. Mydosh, J. Magn. Magn. Mater. **15**, 99 (1980).

[5]See Fig. 14 in H. Lohneysen, Phys. Rep. **79**, 161 (1981); Fig. 4 in H. Lohneysen and J. L. Tholence, Z. Phys. B **29**, 319 (1978).

[6]The data in Fig. 1 of M. B. Salamon and J. L. Tholence, J. Magn. Magn. Mater. **31-34**, 1375 (1983), also appear to exhibit a significant T-independent region for fields greater than 200 G in the amorphous spin glass $Fe_{10}Ni_{20}P_{20}$.

[7]R. V. Chamberlain, M. Hardiman, L. A. Turkevich, and R. Orbach, Phys. Rev. B **25**, 6720 (1982), measured the temperature derivative of the magnetization of Cu-Mn alloys for samples in fixed dc fields. In the vicinity of T_g^0 they found common temperature regions where dM/dT was zero for several field values. This, in turn, implies that there should be regions where $d^2M/dTdH=0$, or since $\chi=dM/dH$, that $d\chi/dT=0$. They attempted to demonstrate this condition in subsequent ac experiments [R. Orbach (private communication)]. We note that the onset temperature where dM/dT first becomes zero, which they suggest may be the AT transition temperature, cannot be simply identified with the cusp-line feature of Fig. 4.

[8]We believe it is important to point out the difference between the data of Fig. 1 and that of Ref. 5 with respect to the flat, T-independent region. For Cu-Mn, as shown by the data of Fig. 1, a flat region is easily discerned for fields greater than 400 G, where the reduction in χ^0 is only $\approx 15\%$. In contrast, for the material of Ref. 5, when a T-independent region is achieved (≈ 1000 G), the entire cusp has been essentially suppressed. A T-independent region at modest fields appears to be observed in $Fe_{10}Ni_{20}P_{20}$ as noted in Ref. 6.

[9]The curvature in Cu-Mn occurs at higher fields than that of Fig. 1. See our Figs. 8 and 9. The curvature for the materials used in Refs. 5 and 6 occur at fields less than 1 kG.

[10]A. P. Malozemoff and Y. Imry, J. Magn. Magn. Mater. **31-34**, 1425 (1983).

[11]Biomagnetic Technologies, Inc., San Diego, California.

[12]G. Toulouse and M. Gabay, J. Phys. (Paris) Lett. **42**, L103 (1981); M. Gabay and G. Toulouse, Phys. Rev. Lett. **47**, 201 (1981).

[13]A. Fert and P. M. Levy, Phys. Rev. Lett. **44**, 1538 (1980).

[14]D. J. Thouless, P. W. Anderson, and R. G. Palmer, Philos. Mag. **35**, 593 (1977).

[15]Our data for the field dependence of the dc magnetization are not shown, but are similar to that of Ref. 2.

[16]D. Sherrington and S. Kirkpatrick, Phys. Rev. Lett. **35**, 1792 (1975).

[17]G. Parisi, Phys. Rev. Lett. **23**, 1754 (1979); D. Sherrington, *Proceedings Heidelberg Colloquium on Spin Glasses,* Vol. 192 of *Lecture Notes in Physics* (Springer-Verlag, Berlin, 1983).

[18]In Appendix B we show that if $P(J_{ij})$ is a Gaussian random distribution, then $P(H_i)$ is also a Gaussian distribution.

[19]J. R. L. de Almeida and D. J. Thouless, J. Phys. A **11**, 983 (1978).

[20]Dinah M. Cragg, D. Sherrington, and M. Gabay, Phys. Rev. Lett. **49**, 158 (1982).

[21]G. Toulouse, M. Gabay, T. C. Lubensky, and J. Vannimenus, J. Phys. (Paris) Lett. **43**, L109 (1982).

[22]M. Gabay, T. Garel, and C. de Dominicis, J. Phys. C **15**, 7165 (1982).

[23]N. de Courtenay, A. Fert, and I. A. Campbell, Phys. Rev. B **30**, 6791 (1984).

[24]G. Kotliar and H. Sompolinsky, Phys. Rev. Lett. **53**, 1751 (1984).

[25]P. Omar *et al.*, J. Phys. (Paris) **44**, 1069 (1983).

[26]H. Bouchiat and P. Monod, in *Proceedings of the International Conference on Magnetism, San Francisco, 1985,* edited by J. J. Rhyne (North-Holland, Amsterdam, 1985).

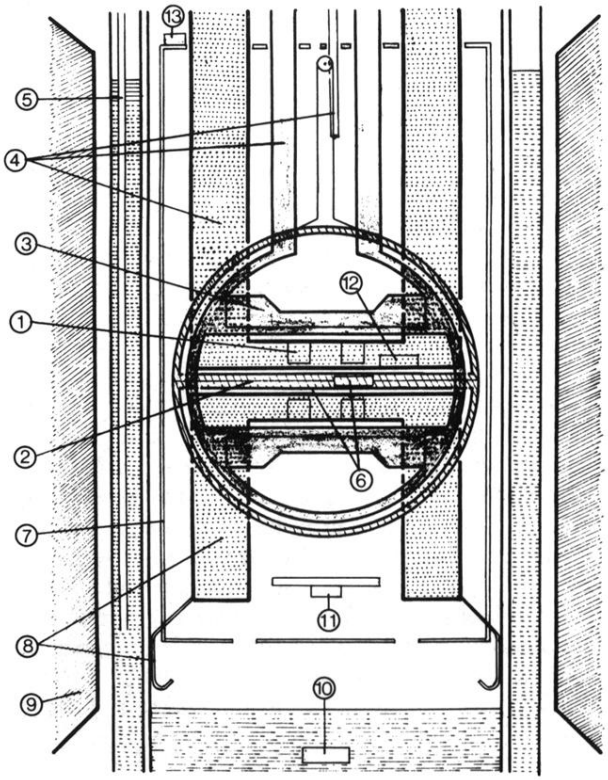

FIG. 5. Detailed scale drawing of the coils and sample arrangement: (1) the astatically wound pickup coils; (2) fine string used to push and/or pull the sample between the two coils of (1); (3) the primary ac coil, coaxial to (1); (4) Various parts of the support system to hold coils firmly in helium Dewar; (5) a fine gas tube in liquid-nitrogen jacket through which gas is blown to reduce bubbling; (6) sample holder containing rolled foil sample which slides in plastic tube; (7) thermal shield made of fine wires and epoxy to eliminate eddy current effects; (8) massive plastic holder with spring fingers to reduce vibration in helium Dewar; (9) external dc magnetic field, varian rotatable magnet with 4-in. gap; (10) heater in liquid helium to produce cooling vapor; (11) heater on thermal shield to regulate temperature; (12) cryogenic thermometer; (13) additional heater to maintain shield at desired uniform temperature.